

## VISUAL ORBIT OF THE LOW-MASS BINARY GJ 164 AB

FRANTZ MARTINACHE<sup>1</sup>, BARBARA ROJAS-AYALA<sup>1</sup>, MICHAEL J. IRELAND<sup>2</sup>, JAMES P. LLOYD<sup>1</sup> AND PETER G. TUTHILL<sup>2</sup>

*Draft version November 5, 2018*

### ABSTRACT

We report seven successful observations of the astrometric binary GJ 164 AB system with aperture masking interferometry. The companion, with a near infrared contrast of 5:1 was detected beyond the formal diffraction limit. Combined with astrometric observations from the literature, these observations fix the parallax of the system, and allow a model-independent mass determination of both components. We find the mass of GJ 164B to be  $0.086 \pm 0.007 M_{\odot}$ . An infrared spectroscopic study of a sample of M-Dwarfs outlines a method for calibrating metallicity of M-Dwarfs. Results from the newly commissioned TripleSpec spectrograph reveal that the GJ 164 system is at least of Solar metallicity. Models are not consistent with color and mass, requiring a very young age to accommodate a secondary too luminous, a scenario ruled out by the kinematics.

*Subject headings:* binary, stars: luminosity functions, mass functions, techniques: AO, interferometric

### 1. INTRODUCTION

The development of a self-consistent theory of the internal structure of stars and the construction of models which trace evolutionary behaviour are major achievements of modern astrophysics. Both theory and models have however long been centered on intermediate and high mass stars, with little consideration of objects with masses below  $0.6 M_{\odot}$ . The realization that the Solar neighborhood is overwhelmingly dominated by low mass stars (van de Kamp 1971; Henry 1998), and the discovery of brown dwarfs (Nakajima et al. 1995) have brought a lot more attention to the lower end of the main sequence and what lies below.

The complex physical nature of these very low mass objects makes their modeling intricate. Boundaries between stars, brown dwarfs and planets, as well as theoretical relations that predict the luminosity and temperature as functions of age, mass and metallicity are still largely untested in the relevant range of parameters. Correct calibration of these models is of extreme importance, since they are now extrapolated to estimate the mass of brown dwarfs (Burrows et al. 2006) and giant exoplanets (Baraffe et al. 2003) from their luminosity and age.

The observations required to challenge and improve the models are dynamical mass measurements of multiple star systems, combined with accurate photometry and distance determination. Besides gravitational microlensing (Paczynski 1986), the observation of binary systems and the use of Newtonian orbital dynamics provide the only method of directly measuring accurate stellar masses. With maximum sensitivity at separations greater than 1 arcsec, conventional Adaptive Optics (AO) observations at Palomar are limited to the most nearby objects or the consequent orbital periods become too long to lead to dynamical masses. We have therefore been using aperture masking interferometry (Tuthill et al. 2000) in conjunction with AO (Lloyd et al. 2006). The precision calibration of the data

achieved with this observing mode indeed leads to reliable results up to and beyond the formal diffraction limit (super resolution), and very precise photometry. Combined with radial velocity (Martinache et al. 2007) or astrometry (Ireland et al. 2008), aperture masking interferometry has so far provided some of the most precise (dynamical) masses of objects below  $0.1 M_{\odot}$ .

### 2. CHARACTERIZATION OF THE ORBIT

We report here aperture masking interferometry observations of the astrometric binary GJ 164 AB. GJ 164 (aka LHS 1642, G 175-19 or Ross 28) is a high proper motion star, catalogued as a M4.5 Dwarf (Reid et al. 1995), 11-13 pc distant. From the 2MASS catalog, its apparent near infrared magnitudes are  $J = 8.773 \pm 0.032$ ,  $H = 8.248 \pm 0.030$ , and  $K = 7.915 \pm 0.016$ . The discovery of GJ 164 B was reported by Pravdo et al. (2004), as a part of the STEPS program of Pravdo & Shaklan (1996). The combination of the astrometry data from the discovery paper, combined with the aperture masking interferometry data reported in this paper provides a complete dynamical characterization of the system, resulting in masses that are independent of the use of a model or a mass-luminosity relation. GJ 164 is an especially interesting target for the mass of the B component lies very close to the substellar limit.

#### 2.1. Aperture Masking Interferometry

Measuring the dynamical masses of a low-mass binary system requires some patience, for the observations have to cover at the very least a significant fraction of the orbital period. Because of its low mass ( $< 0.6 M_{\odot}$ ), a relatively short period ( $< 10$  yr) binary will have a semimajor axis smaller than 4 AU. Even for objects as close as 10 parsecs, the angular separation won't exceed 0.4 arcsecs, a performance theoretically within the grasp of a 5-10 meter class telescope equipped with AO. Yet in practice, the residual quasi-static speckles in the AO PSF halo seriously limit the capability of detecting a companion at angular separation smaller than 2-4  $\lambda/D$  (Racine et al. 1999). Aperture masking interferometry with AO addresses this issue.

A non redundant mask discards most of the pupil by

<sup>1</sup> Department of Astronomy, Cornell University, Ithaca NY

<sup>2</sup> School of Physics, University of Sydney, Sydney NSW Australia

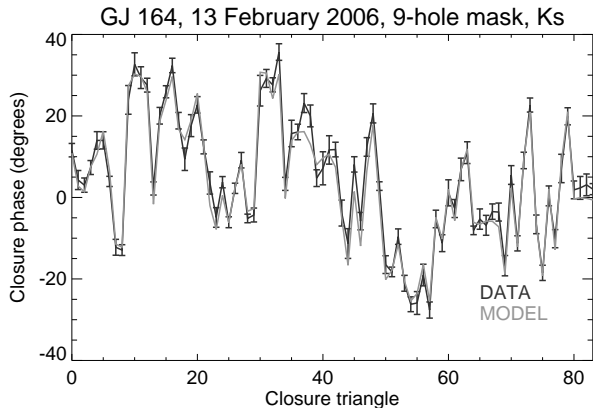


FIG. 1.— Calibrated closure phases observed on JD 2453779.71 with a  $K_S$  filter. A binary star model (light gray) with a 86 mas separation, a position angle of  $102^\circ$  and a contrast of 5:1 satisfactorily matches the observations (dark gray).

sampling a few spatial frequencies only (Readhead et al. 1988; Naka-jima et al. 1989). One admittedly loses most of the light (the 9-hole mask used for this work transmits approximately 15 %) but rejects all atmospheric noise, as well as internal aberrations and non common path errors, which in turn, dramatically increases the signal-to-noise ratio (Tuthill et al. 2000). Used in conjunction, aperture masking interferometry and AO provide stable fringes, and enable long integration times, therefore making faint target accessible. The only limit is whether the AO system can lock on the system. Thus, any target that can be observed with AO can also be observed with aperture masking interferometry. With a visible magnitude  $V = 13.5$  (Weis 1996), GJ 164 can fairly easily be observed with aperture masking. If calibration is sufficiently accurate, the interferometry enables super-resolution, ie. the detection of structures on a target at a scale smaller than  $\lambda/D$ . The data presented in Tables 1 and 2 shows that the companion to GJ 164 A is detected on multiple occasions in that super-resolution regime. Tuthill et al. (2006) provide a recent description of the general principles and performances of aperture masking interferometry while Lloyd et al. (2006) detail the experiment undertaken at Palomar.

The AO observations performed with PHARO (Hayward et al. 2001) at Palomar as well as with NIRC2 at Keck II span the range December 2003 to December 2006. The companion was successfully detected all seven runs. The data are calibrated with observations of one or several stars of similar brightness for both the AO wave front sensor and the science camera to ensure comparable wave front correction and signal-to-noise ratio. The final dataproducit of our custom software pipeline written in IDL, is a collection of calibrated closure phases (Baldwin et al. 1986). This very robust observable rejects both atmospheric noise and calibration errors of the wave front sensor. The 9 hole mask provides  $\binom{9}{3}=84$  possible closure triangles,  $\binom{8}{2} = 28$  of which are theoretically independent.

The instantaneous geometry of a binary star is modeled by a set of three parameters: contrast ratio  $c$ , angular separation  $a$  and position angle (PA)  $\theta$ . The example of one such model fitted to a set of closure phases is given in Figure 1. The aperture masking data processing software typically uses several hundreds of frames which are

TABLE 1  
APERTURE MASKING MEASUREMENTS AT  
PALOMAR AND KECK: ANGULAR SEPARATION AND  
POSITION ANGLE OF GJ 164 B.

Julian Date (-2,450,000)	Band	Telescope	Sep.	PA
3004.85	H	Palomar	$82.8 \pm 1.6$	$111.1 \pm 0.9$
3632.96	H	Palomar	$53.3 \pm 1.3$	$149.1 \pm 1.2$
3723.66	H	Palomar	$80.1 \pm 3.3$	$116.1 \pm 2.1$
3779.71	H, $K_S$	Palomar	$86.1 \pm 2.0$	$102.1 \pm 0.9$
3957.62	H	Keck	$49.3 \pm 0.5$	$47.0 \pm 0.6$
4018.98	$K_S$	Palomar	$39.4 \pm 1.3$	$344.8 \pm 2.6$
4078.79	$K_S$	Palomar	$57.3 \pm 2.2$	$294.1 \pm 2.8$

TABLE 2  
GJ 164 PHOTOMETRY

Julian Date (-2,450,000)	Filter	Contrast
3004.85	H	$5.97 \pm 0.32$
3632.96	H	$5.77 \pm 0.46$
3723.67	H	$5.78 \pm 0.63$
3779.71	H	$5.53 \pm 0.60$
	$K_S$	$4.89 \pm 0.19$
3957.62	H	$5.42 \pm 0.03$
4018.98	$K_S$	$8.66 \pm 4.81$
4078.79	$K_S$	$5.67 \pm 1.17$

averaged to produce the closure phases. Due to the central limit theorem, the distribution of closure phases  $\{\phi_i\}$  can be considered Gaussian, with uncertainties  $\sigma_i$  given by the standard deviation to the mean. The best fit minimizes the traditionally used goodness-of-fit parameter  $\chi^2$  defined as

$$\chi^2 \equiv \sum_i \frac{(\phi_i - f_i(a, \theta, c))^2}{\sigma_i^2}, \quad (1)$$

where  $f_i$  designates the model. A systematic error term is added to the closure phase dispersion  $\sigma_i$  to achieve a reduced  $\chi^2_\nu = 1$ . The likelihood of the parameters given the set of closure phases  $\{\phi_j\}$  is related to the  $\chi^2$  by

$$L(a, \theta, c | \{\phi_j\}) \propto \exp(-\chi^2/2). \quad (2)$$

Normalized,  $L$  is the full joint probability density function for all three parameters. The confidence interval of one individual parameter is calculated by integrating out the two others. For example, the marginal probability density function for the angular separation is calculated by integrating out the position angle and the contrast ratio:

$$p(a) = \int d\theta dc L(a, \theta, c). \quad (3)$$

The results of this analysis: relative position and photometry are gathered in Tables 1 and 2. The more or less favorable seeing conditions explain the variable confidence interval sizes. We achieve a precision of a few milliarcseconds at separations as low as 44 mas in  $K_S$  band ( $0.5 \lambda/d$ ) on good nights at Palomar.

## 2.2. Astrometry

GJ 164 was discovered as a binary in an astrometric survey by Pravdo & Shaklan (1996); Pravdo et al.

TABLE 3  
GJ 164 ASTROMETRY

Julian Date (-2,450,000)	$\Delta$ R.A.	$\Delta$ Decl.
0801.5	0.00	0.00
0801.5	0.00	-2.80
1088.3	-147.91	-646.96
1189.0	-328.82	-874.15
1189.0	-324.82	-874.05
1189.0	-325.32	-871.65
1436.5	-457.34	-1409.82
1494.0	-563.37	-1519.60
2657.5	-1639.04	-4132.08
2889.5	-1745.18	-4629.59
2889.5	-1745.18	-4627.29
2889.5	-1745.88	-4625.69
3030.5	-2014.31	-4953.05
3030.5	-2014.61	-4957.45
3051.5	-2044.87	-5016.85

(2004). While the interferometry resolves the binary and provides its instant geometric configuration, the astrometry records the position of a star’s photocenter, measured relative to several more distant stars. Repeated observations reveal the star’s proper motion as well as its parallax. Once these two effects subtracted from the astrometric signal, any residual wobble of the photocenter can be attributed to the presence of one or more companions, massive enough to cause an observable shift in position. The orbit of the companions can then be fully characterized.

Astrometric data were extracted from the figures of Pravdo et al. (2004) then added the motion due to the proper motion and the parallax given in the paper’s tables. These extracted values are gathered in Table 3. We initially assume a 2.0 mas uncertainty for each individual measurement, as suggested by the residuals of the analysis performed by Pravdo et al. (2004).

The astrometric residual wobble however remains a function of the fractional light of the secondary,  $\beta = L_2/(L_1 + L_2)$ , with  $L_1$  and  $L_2$  respectively denoting the luminosity of the primary and the secondary, as well as the fractional mass of the secondary  $f = m_2/(m_1 + m_2)$ . In the limit at which the light of the secondary is negligible, the photocentric orbit is identical to the Keplerian orbit of the primary around the actual center of mass of the system. If the luminosity of the secondary is not so negligible, then the photocentric semimajor axis  $\alpha$  is reduced proportionally to  $\beta$ . The ratio of the photocentric orbit  $\alpha$ , and the Keplerian orbit  $a$  is (McCarthy et al. 1988):

$$\alpha/a = f - \beta. \quad (4)$$

A relatively small-mass, non-luminous secondary, and a relatively large-mass, luminous secondary will therefore have identical astrometric signatures. The data presented in Section 2.1 however rules out the latter possibility. Indeed, the aperture masking interferometry data gathered in Table 2 provides the H and  $K_S$  band contrast ratios, which are turned into the following differences of magnitude:

$$\begin{aligned} \Delta H &= 1.835 \pm 0.006 \\ \Delta K_S &= 1.721 \pm 0.097. \end{aligned}$$

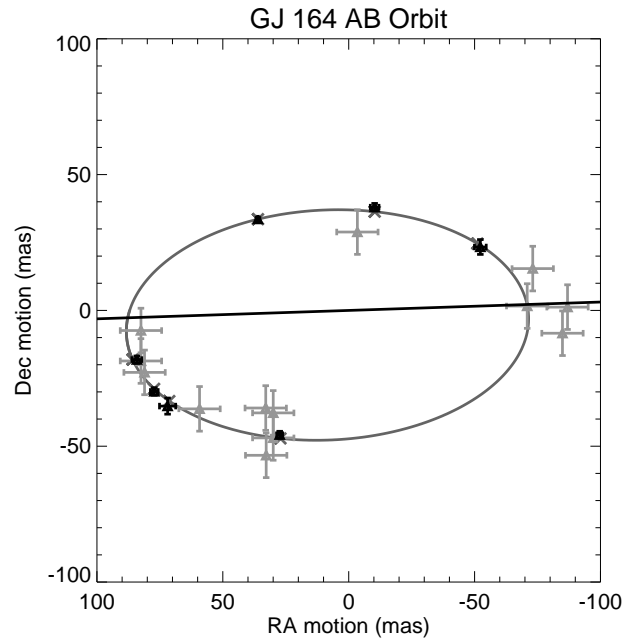


FIG. 2.— GJ 164 B ORBIT. The measurements and associated uncertainties of the Aperture Masking data are represented by dark gray rectangles. Light gray triangles represent the STEPS astrometry data. The relative apparent orbit (curve) is clockwise. Table 4 provides the corresponding orbital elements. The almost horizontal straight line represents the line of nodes.

These contrast ratios can be used to decompose the 2MASS combined magnitudes of the binary into apparent magnitudes for individual components:  $H = 8.432 \pm 0.030$  and  $K = 8.117 \pm 0.017$  for GJ 164A,  $H = 10.267 \pm 0.030$  and  $K = 9.834 \pm 0.038$  for GJ 164B.

The corresponding (H-K) color indices:  $(H - K)_A = 0.315 \pm 0.034$  and  $(H - K)_B = 0.433 \pm 0.048$  alone, provide a parallax-independent observable. While the  $(H - K)$  color index of the primary is well compatible with a M4.5 spectral type, the secondary is very unlikely to be any earlier than M8 (see for instance Koornneef (1983)). A well characterized nearby equivalent is the star VB 10 from the 8 parsec survey (Henry et al. 1994).

We use VB 10 as a standard to estimate the contrast ratio of the two components of GJ 164 in the R band where the astrometry data was taken. The 2MASS catalogue provides a  $(R - K) = 6.8$  color index for VB 10, which combined with the data gives an apparent  $R = 16.6$  magnitude for GJ 164B. Monet et al. (2003) give  $R = 12.4$  for GJ 164A, which corresponds to a contrast ratio  $c \approx 47$ . This gives an upper limit to the fractional light of the secondary:  $\beta = 0.021$ , which means that the hypothesis of a secondary of negligible visible luminosity would, at most, underestimate the mass ratio (cf. eq. 4) by 2.1 %. This systematic uncertainty needs to be added up to the statistical uncertainty deduced from the  $\chi^2$  analysis performed in Section 3.2.

### 3. CHARACTERISTICS OF GJ 164 AB

#### 3.1. Orbital Parameters

The aperture masking observations gathered in Table 1 provide the instant position of the companion to the primary. These observations alone suffice to constrain all seven orbital elements of the binary, independently of the parallax, with the semimajor axis expressed in angular

units.

We use a model identical to the one described in Section 3.1.2 of Martinache et al. (2007) to fit a seven-parameter model to 14 observables. The observables are two coordinates for seven aperture masking data points. The seven orbital parameters are: the angular semimajor axis  $\alpha$ , the eccentricity  $e$ , the longitude of the ascending node  $\omega_0$ , the inclination  $i$ , the argument of the periastron  $\Omega_1$ , the period  $P$  and the epoch at periastron passage  $T_P$ . Our solution exhibits a final reduced  $\chi^2_\nu = 0.61$  for 7 degrees of freedom. Note that the temporal coverage of these observations definitely rules out the possibility of a  $\sim 4$  yr orbital period suggested by Pravdo et al. (2004). The seven orbital parameters and the associated uncertainties are presented in Table 4.

We then proceed to a joined fit AO + astrometry, that is a thirteen-parameter fit to 40 observables. The extra parameters included in this new analysis are: the two components of the proper motion, the relative parallax  $\Pi$  as well as the semimajor axis of the motion of the primary around the center of mass of the system  $a_1$ . With a 2 mas uncertainty on the individual astrometric measurements, as assumed in Pravdo et al. (2004), the solution to this global fit exhibits a final reduced  $\chi^2_\nu = 0.73$  for 27 degrees of freedom. We therefore assumed astrometric errors of 1.4 mas so that the reduced  $\chi^2_\nu$  is exactly 1. Table 4 compares the seven orbital parameters and their uncertainties obtained from the fit of the AO data only and the joined fit: both approaches produce compatible solutions. Figure 2 represents the orbit resulting from this joined fit, onto which are superposed the AO and astrometry data.

### 3.2. Dynamical Masses

Like Pravdo et al. (2004), we use a  $2 \pm 1$  mas correction to convert the relative parallax  $\Pi = 70.0 \pm 0.8$  mas, to the absolute parallax:  $\Pi = 72.0 \pm 1.2$  mas. We can now determine the actual relative semimajor axis of the binary:  $a = 1.1 \pm 0.2$  AU, as well as the total mass:

$$M_T = a^3/P^2, \quad (5)$$

that is  $M_T = 0.343 \pm 0.026 M_\odot$ . In the limiting case where the luminosity of the secondary is negligible, the fractional mass of the secondary (cf. eq. 4) is given by the ratio of the photocentric and relative orbit semimajor axis, that is  $f = 0.250 \pm 0.010$ . It is remarkable that the fractional mass should be a ratio of two angular radii, for this makes this quantity parallax-independent. Section 2.2 shows there is at least a 3.8 magnitude difference between the two components of the binary, which translates into a fractional light  $\beta = 0.021$ . The fractional mass  $f$  therefore requires non symmetric uncertainties:  $f = 0.250^{+0.031}_{-0.010}$ .

From the total mass and the fractional mass, one can infer the masses of both components:  $M_2 = 0.086^{+0.012}_{-0.007}$  and  $M_1 = 0.257^{+0.020}_{-0.022}$ . All dynamical characteristics of the GJ 164 system are given in Table 6.

## 4. SPECTROSCOPY

Careful characterization of the atmosphere and determination of abundances is necessary to understand the location of GJ 164 AB in a mass-luminosity (M/L) diagram, relative to an observational M/L relation or to nu-

TABLE 4  
ORBITAL ELEMENTS

Parameter	AO only	AO + STEPS
$\alpha$ (mas)	$80.4 \pm 1.3$	$80.5 \pm 1.2$
$e$	$0.157 \pm 0.012$	$0.161 \pm 0.012$
$i$ (deg)	$121.9 \pm 0.9$	$121.9 \pm 0.8$
$\Omega_1$ (deg)	$272.4 \pm 1.3$	$271.8 \pm 1.2$
$\omega_o$ (deg)	$314.7 \pm 5.0$	$311.7 \pm 3.7$
$P$ (days)	$734.3 \pm 4.6$	$736.9 \pm 1.7$
$T_P$ (reduced JD)	$1868 \pm 19$	$1856 \pm 8$

TABLE 5  
ASTROMETRIC ELEMENTS

Parameter	Value
Proper motion R.A. (mas)	$-324.5 \pm 0.3$
Proper motion Decl. (mas)	$-808.3 \pm 0.3$
Relative Parallax (mas)	$70.0 \pm 0.8$
Phot. semimaj. axis (mas)	$20.1 \pm 0.8$
Total Mass ( $M_\odot$ )	$0.343 \pm 0.026$

TABLE 6  
DYNAMICAL MASSES: OBTAINED FROM THE  
JOINED ANALYSIS AO+STEPS. SEE TEXT FOR  
MORE DETAILS ON UNCERTAINTIES!

Parameter	Value
Total Mass	$M_T = 0.343 \pm 0.026 M_\odot$
Primary Mass	$M_1 = 0.257 \pm 0.020 M_\odot$
Secondary Mass	$M_2 = 0.086 \pm 0.007 M_\odot$
Mass ratio	$M_2/M_T = 0.250 \pm 0.010$

merical simulations of M-Dwarf atmospheres. Determining the overall metallicity of mid-to-late type M-Dwarfs is however a delicate task. Indeed, with  $(V-K) > 5$  for spectral types later than M-4, optical spectroscopy doesn't appear as an efficient approach, while in the infrared, there is no well-established proxy for metallicity that calibrates with its optical counterpart.

One strategy to solve this problem is to observe binary systems where the primary is a Solar-type star (F,G or K-Dwarf) of known metallicity and the secondary a M-Dwarf. Assuming that both components formed from the same original molecular cloud, they should share the same metallicity. In the context of addressing the planet-metallicity correlation for M-Dwarf planet surveys (Edelstein et al. 2007; Muirhead et al. 2008) we have begun a separate study of a population of such objects (Rojas-Ayala & Lloyd 2008). Initial results from this study and its conclusions for the metallicity of GJ 164 are presented in this section.

### 4.1. Observations and Data Reduction

Our spectroscopic sample consists of five M4-5-Dwarfs (in complement to GJ 164 AB) associated to Solar type stars, whose metallicity was measured by Valenti & Fischer (2005). Their designation, spectral type, V and K apparent magnitudes, as well as metallicities are listed in Table 7.

Near-infrared spectra of these objects were obtained with the recently commissioned TripleSpec spectrograph on the Palomar Hale Telescope (Wilson et al. 2004; Herter et al. 2008). TripleSpec at Palomar is a  $\lambda/\Delta\lambda$

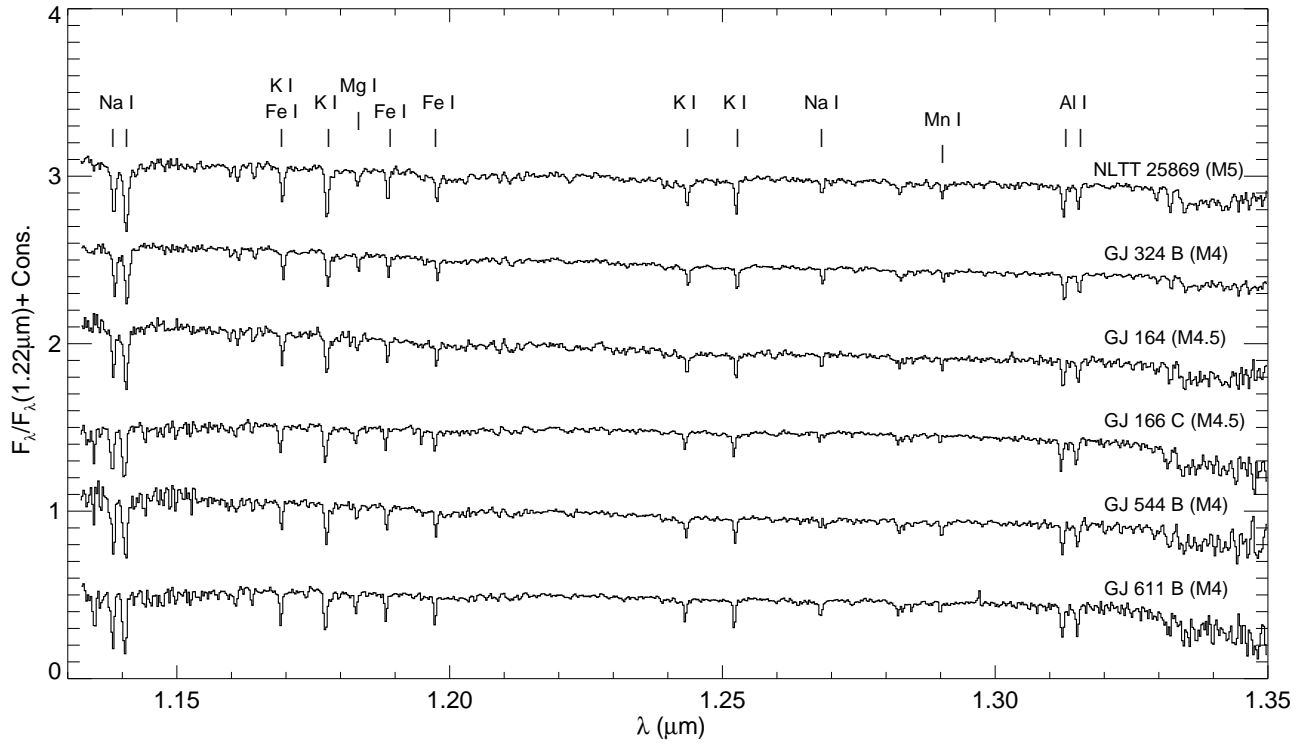


FIG. 3.— J-band spectra of the stars ordered from top to bottom by decreasing metallicity (listed in Table 7). The most prominent spectral features are highlighted.

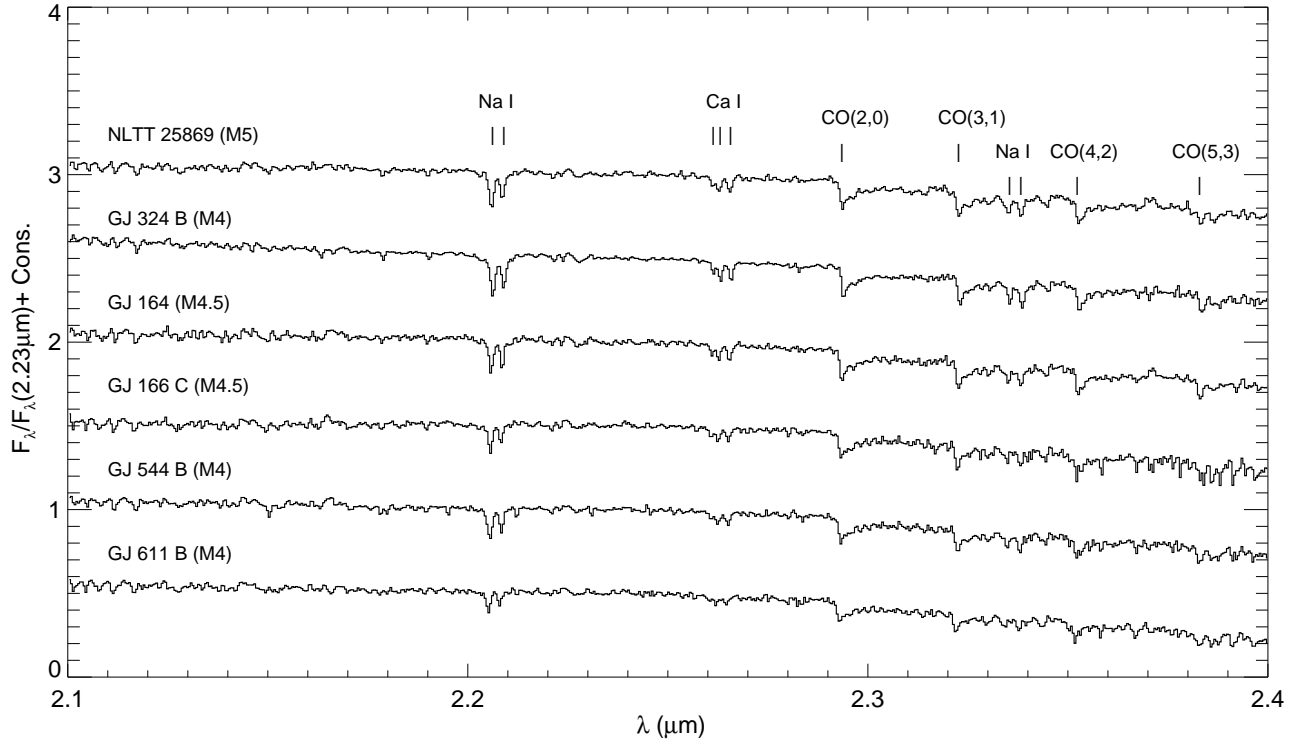


FIG. 4.— K-band spectra of the stars ordered from top to bottom by decreasing metallicity (listed in Table 7). The most prominent spectral features are highlighted.

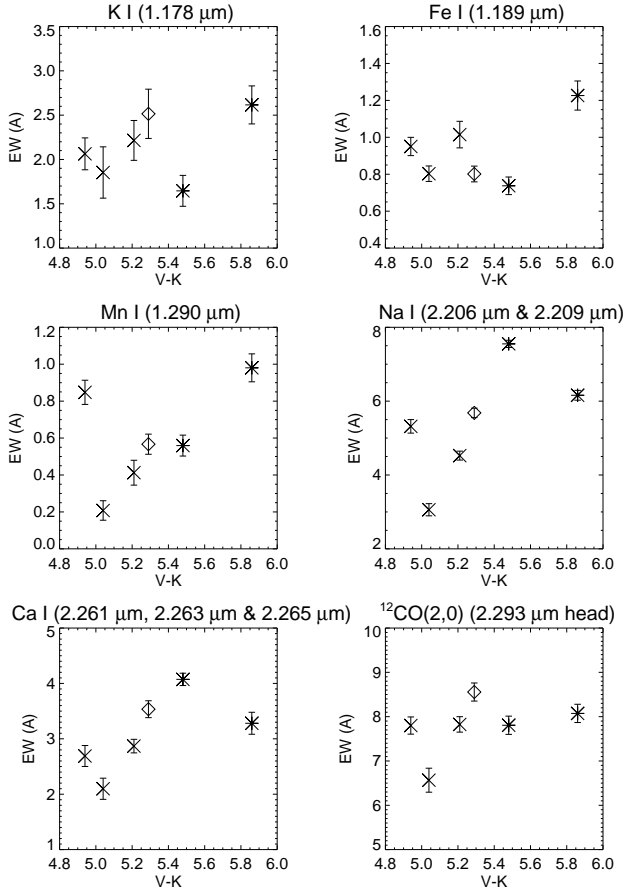


FIG. 5.— Equivalent widths of some of the most prominent lines in the sample spectra with  $1\sigma$  errors versus (V-K) colors. A diamond represents GJ 164 AB, metal-rich objects ( $[M/H] > 0.0$ ) are represented by asterisks and metal-poor objects ( $[M/H] < 0.0$ ) by crosses.

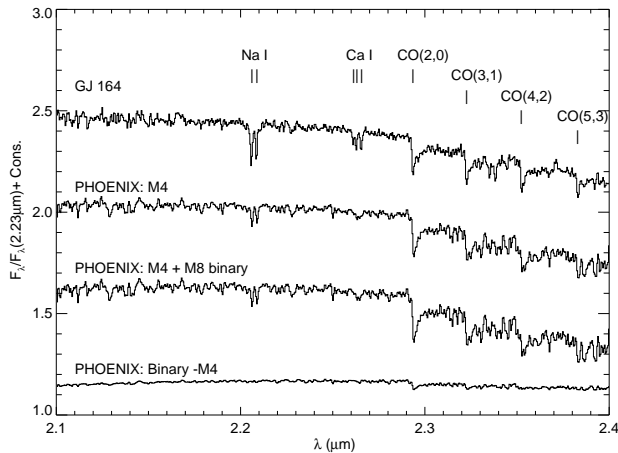


FIG. 6.— Spectrum of GJ 164 (top) compared to the PHOENIX models of Hauschildt et al. (1999) for Solar metallicity: the models (labeled PHOENIX:M4) reproduce most features of the spectrum. The presence of a M8-Dwarf companion with a 5:1 K-band contrast ratio (labeled PHOENIX:M4+M8) only modifies the strength of the CO bands, as shown in the plot of the difference between the two models (bottom).

TABLE 7  
THE SAMPLE

Name	Sp. Typ.	V [mag]	K [mag]	$[M/H]$ dex
GJ 324 B	M4	13.15	7.67	$+0.25 \pm 0.03$
GJ 544 B	M4	14.50	9.59	$-0.15 \pm 0.03$
GJ 611 B	M4	14.20	9.16	$-0.49 \pm 0.03$
GJ 166 C	M4.5	11.17	5.96	$-0.08 \pm 0.03$
NLTT 25869	M5	14.50	8.64	$+0.27 \pm 0.03$

$\approx 2500$ - $2700$  cross-dispersed near-infrared spectrograph with a broad wavelength coverage across 5 simultaneous orders ( $1.0$ - $2.4 \mu\text{m}$ ) in echelle format. Its entrance slit is  $1 \times 30$  arcseconds and a notable feature is that it has no moving parts.

The data were reduced with an IDL-based data reduction pipeline developed by P. Muirhead for TripleSpec at Palomar. The data were sky-subtracted using a sky-frame made by median combination of the 5 exposures on different positions along the slit of the object. To correct for telluric absorption features and flux-calibrate their spectra, an A0 V star was observed as close to the science object star airmass as possible. Each sky-subtracted exposure was then divided by a normalized flat-field, wavelength calibrated and fully extracted. The spectra are flux-calibrated and telluric corrected using the IDL-based code `xtellcor_general` described in the paper by Vacca et al. (2003).

The final J- and K-band spectra along with the most prominent features are shown in Figs. 3 and 4, respectively.

#### 4.2. Equivalent Widths

The equivalent width (EW) of six prominent features in the J and K-band spectra were estimated using the the IDL-based function `measure_ew` by N. Konidaris and J. Harker. Each spectrum was normalized and the equivalent widths were calculated by computing the ratio of the area of a feature to a pseudocontinuum. This pseudocontinuum is a linear interpolation of clean regions on either side of the feature. Uncertainties in the equivalent width were obtained using the procedure described in Sembach & Savage (1992).

The equivalent widths of K I ( $1.178 \mu\text{m}$ ), Fe I ( $1.189 \mu\text{m}$ ) and Mn I ( $1.290 \mu\text{m}$ ) in J-band as well as Na I ( $2.206 \mu\text{m}$  &  $2.209 \mu\text{m}$ ), Ca I ( $2.261 \mu\text{m}$ ,  $2.263 \mu\text{m}$  &  $2.265 \mu\text{m}$ ) and  $^{12}\text{CO}(2,0)$  ( $2.293 \mu\text{m}$ ) in K-band are shown in Fig. 5. Crosses depict the stars with  $[M/H] < [M/H]_{\odot}$  (GJ 544 B, GJ 611 B and GJ 166 C) and asterisks depict the stars with  $[M/H] > [M/H]_{\odot}$  (GJ 324 B and NLTT 25869). A diamond represents GJ 164 AB.

#### 4.3. Metallicity of GJ 164

Except for the Fe I lines that do not exhibit any correlation with spectral type (Cushing et al. 2005), most of the spectral features shown in Fig. 5 are strongly temperature-dependent (Ali et al. 1995; Jones et al. 1996). The dispersion in EW between objects with roughly the same temperature and gravity will therefore provide insights on the metal abundances, and the spectrum of GJ 164 shows features of strength comparable to the metal-rich stars of our sample, especially in K-band (cf. Fig. 4). Except for K I ( $1.178 \mu\text{m}$ ) and

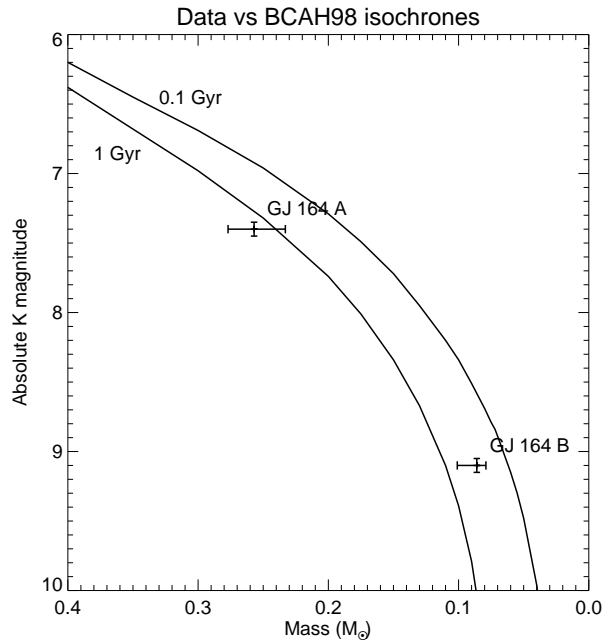


FIG. 7.— GJ 164 A and B in a Mass-Luminosity diagram. The absolute K magnitudes are compared to the BCAH98 isochrones for 0.1 and 1.0 Gyr. Asymmetric confidence intervals on the masses of both components are due to the uncertainty on the contrast ratio at the wavelength where the astrometry was taken.

Fe I (1.189  $\mu\text{m}$ ), the EW of its lines (cf. Fig. 5) make GJ 164 more likely to be metal-rich than metal-poor.

The high value of GJ 164’s  $^{12}\text{CO}(2,0)$  (2.293  $\mu\text{m}$ ) EW (Fig. 5, bottom right panel) can be attributed to its secondary. Indeed, the data presented in Section 2.1 shows that the contrast ratio between GJ 164 A (M4) and GJ 164B (M8) is close to 5:1 in K. Since the strength of the CO bands increases with later types in the M-Dwarf sequence, GJ 164 B (unresolved with TripleSpec) adds a non-negligible contribution to the strength of these molecular features. Figure 6 compares the K-band spectrum of GJ 164 to PHOENIX spectra (Hauschildt et al. 1999). A M4-Dwarf spectra alone as well as a spectrum composed of a M4 and a M8 with a 5:1 contrast ratio, all for  $[M/H]=0.0$ . Although the strength of the Na I doublet and the Ca I triplet in the PHOENIX spectra differ from our data, the strengths and shapes of the CO bands predicted by the models match the spectra of GJ 164. The difference between these two spectra at the bottom of Fig. 6 shows that the only features affected by the M8 companion at these wavelengths are the CO bands.

## 5. MASS-LUMINOSITY RELATIONS

The individual apparent magnitudes calculated in Section 2.2, combined with the absolute parallax deduced from the dynamical analysis performed in Section 3.2, determine the following absolute H and K magnitudes:  $M_H = 7.721 \pm 0.051$  and  $M_K = 7.407 \pm 0.047$  for GJ 164 A,  $M_H = 9.557 \pm 0.051$  and  $M_K = 9.128 \pm 0.047$  for GJ 164 B.

The (H-K) colors, corroborated by the infrared spectroscopy data presented in Section 4 indicate that GJ 164 is at least of Solar metallicity. Figure 7 compares the location of GJ 164 A and B in a Mass-luminosity diagram, relative to the low-mass Solar metallicity models

of Baraffe et al. (1998) (hereafter referred to as BCAH98) for the K-band. For masses below  $0.4 M_\odot$  (but above the substellar limit), models predict very little evolution between 0.5 and 5 Gyr. Fig. 7 therefore only plots two isochrones, for 0.1 and 1 Gyr.

The aperture masking data places the primary less than  $1-\sigma$  away from the 1 Gyr isochrone, and  $3-\sigma$  away in mass from the 0.1 Gyr isochrone. The hypothesis of an evolved age is supported by the kinematics of the system. Indeed, with the proper motion  $(-324.5, -808.4)$  mas  $\text{yr}^{-1}$ , the absolute parallax  $\Pi = 72 \pm 1.2$  mas derived in Section 3.2, as well as the radial velocity  $V = -29.9$  km  $\text{s}^{-1}$  measured by Pravdo et al. (2004), one can calculate the Galactic space velocity  $(U, V, W) = (-24, -20, -47)$  km  $\text{s}^{-1}$  after correction for standard solar motion.<sup>3</sup> When compared to the properties of the nearest young moving groups (cf. Table 1 of López-Santiago et al. (2006)), GJ 164 exhibits a velocity component perpendicular to the Galactic plane too large to be associated to any of these groups. From the kinematic properties of the M-Dwarf survey of Reid et al. (2002), it is however impossible to conclude whether GJ 164 belongs to the thin or the thick disk.

The case of GJ 164 B is a little bit more puzzling. Indeed, as the mass decreases, the luminosity predicted by the models becomes a very steep function of the mass. GJ 164 B lies  $1.5 \sigma$  away from the 1 Gyr isochrone horizontally, which is only marginally in conflict with the models. However, based on these dynamical mass and luminosity measurements, the models underestimate the luminosity of a  $<0.1 M_\odot$  star by roughly one magnitude. A way to accommodate for this discrepancy would be for the GJ 164 A to be a tight binary, like for example the case of GJ 802 exposed in Ireland et al. (2008). Spectroscopic observations by Pravdo et al. (2004) however showed no evidence that GJ 164 A is a spectroscopic binary.

To provide a stronger case, Figure 8 plots more of the BCAH98 isochrones (0.1, 0.2, 0.3, 0.5 and 1 Gyr), this time in the plane mass ratio  $f$  (cf. eq. 4), against the K-band magnitude difference.  $\Delta K$  is a direct measurement made with the aperture masking interferometry data (cf. Table 2) while  $f$  is a derived product of the joined fit, obtained in Section 3.2. Both observables are parallax-independent, which makes them more robust than the individual masses and luminosities.

Although taking into account all the uncertainties of our analysis by generating families of models within  $\pm 1$  standard deviation of the total mass of the binary, the  $1.5-\sigma$  discrepancy between the data and the models presented in Fig. 7 now turns out to be over  $5 \sigma$  away from the 1 Gyr isochrone: the models presented in Fig. 8 clearly favor a very young age (100 Myr), which accommodates for the apparent excessive luminosity of GJ 164 B, but is incompatible with the kinematics of the system. Note that the same conclusion holds when performing a similar analysis using H-band mass-luminosity relations.

## 6. CONCLUSION

<sup>3</sup> The sign convention is the one of the IDL astrolib gal\_uv procedure, with U positive toward the Galactic anti-center, V positive in the direction of Galactic rotation, and W positive toward the North Galactic Pole.

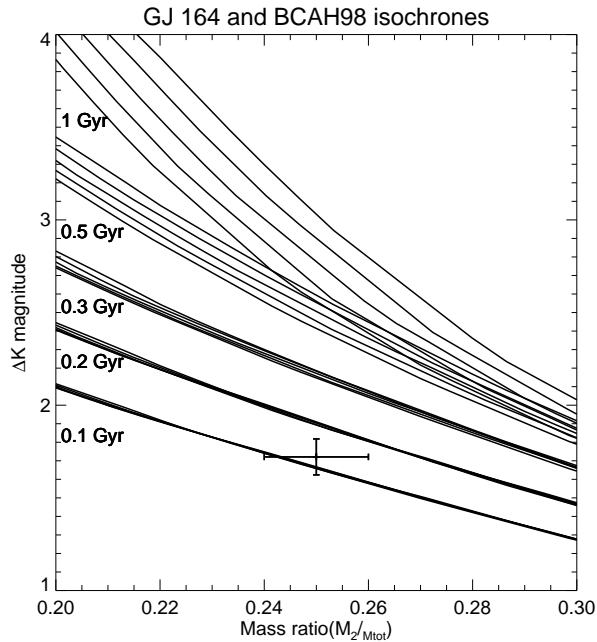


FIG. 8.— The mass ratio and K-band contrast ratio of GJ 164 (datapoint of coordinates (0.25, 1.8)) are compared to BCAH98 isochrones for ages between 0.1 and 1 Gyr. Each age generates a family of models taking into account the uncertainty on the total mass of the binary.

GJ 164 is an astrometric binary, whose orbit was resolved by aperture masking interferometry observations at Palomar and Keck. The consistency of the data is excellent, and exhibits a 1-2 mas precision in average for each measurement, made below what is usually accepted as the resolution limit of a telescope. This data, combined with earlier astrometric measurements, provides the following dynamical masses:  $0.257 \pm 0.020 M_{\odot}$  for the primary and  $0.086 \pm 0.007 M_{\odot}$  for the secondary.

Analysis of its infrared spectrum reveals that the M-Dwarf binary GJ 164 is at least of Solar metallicity. When attempting to use theoretical models for Solar metallicity very low-mass stars to derive an age from

the mass and luminosity of both components, we find that the models do not adequately fit the data, requiring very young ages to accommodate for an overluminous secondary. The models therefore underestimate the luminosity of very low-mass stars that have settled on the main sequence.

The precision of the dynamical data we present here, of the order of 10 percents, however does not provide a strong constraint for the models. A precise measurement of the contrast ratio in the R band, where the astrometry data was taken would already help to better constrain the mass ratio and ultimately improve the constraint on the individual masses, and make our statement about the models stronger. The very small separation (at most, 90 mas) makes this measurement difficult, even for HST. But because it lies so close from the substellar limit, GJ 164 B is a target that deserves most attention. In the meantime, a Radial Velocity curve would provide an independent measurement of the mass ratio. With an expected Radial Velocity amplitude of 2.8 km/sec, and a period of two years, observations of GJ 164 with Triple-Spec and TEDI will settle this uncertainty.

We thank the staff and telescope operators of Palomar Observatory and Keck Observatory for their support. B. Rojas-Ayala thanks Travis Barman for providing the PHOENIX models used for this work. This work is partially funded by the National Science Foundation under grants AST-0504874 and AST-0705085. This publication makes use of the Simbad database, operated at CDS, Strasbourg, France and the data products from the Two Micron All Sky Survey, which is a joint project of the University of Massachusetts and the Infrared Processing and Analysis Center/California Institute of Technology, funded by the National Aeronautics and Space Administration and the National Science Foundation. We wish to extend special thanks to those of Hawaiian ancestry on whose sacred mountain we are privileged to be guests. Without their generous hospitality, the observations presented herein would not have been possible.

#### REFERENCES

- Ali, B., Carr, J. S., Depoy, D. L., Frogel, J. A., & Sellgren, K. 1995, *AJ*, 110, 2415
- Baldwin, J. E., Haniff, C. A., Mackay, C. D., & Warner, P. J. 1986, *Nature*, 320, 595
- Baraffe, I., Chabrier, G., Allard, F., & Hauschildt, P. H. 1998, *A&A*, 337, 403
- Baraffe, I., Chabrier, G., Barman, T. S., Allard, F., & Hauschildt, P. H. 2003, *A&A*, 402, 701
- Burrows, A., Sudarsky, D., & Hubeny, I. 2006, *ApJ*, 640, 1063
- Cushing, M. C., Rayner, J. T., & Vacca, W. D. 2005, *ApJ*, 623, 1115
- Edelstein, J., Muterspaugh, M. W., Erskine, D. J., Feuerstein, W. M., Marckwordt, M., Wishnow, E., Lloyd, J. P., Herter, T., Muirhead, P., Gull, G. E., Henderson, C., & Parshley, S. C. 2007, in Presented at the Society of Photo-Optical Instrumentation Engineers (SPIE) Conference, Vol. 6693, Techniques and Instrumentation for Detection of Exoplanets III. Edited by Coulter, Daniel R. Proceedings of the SPIE, Volume 6693, pp. 66930W-66930W-6 (2007).
- Hauschildt, P. H., Allard, F., & Baron, E. 1999, *ApJ*, 512, 377
- Hayward, T. L., Brandl, B., Pirger, B., Blacken, C., Gull, G. E., Schoenwald, J., & Houck, J. R. 2001, *PASP*, 113, 105
- Henry, T. J. 1998, in ASP Conf. Ser. 134: Brown Dwarfs and Extrasolar Planets, ed. R. Rebolo, E. L. Martin, & M. R. Zapatero Osorio, 28–
- Henry, T. J., Kirkpatrick, J. D., & Simons, D. A. 1994, *AJ*, 108, 1437
- Herter, T. L., Henderson, C. P., Wilson, J. C., Matthews, K. Y., Rahmer, G., Bonati, M., Muirhead, P. S., Adams, J. D., Lloyd, J. P., Skrutskie, M. F., Moon, D.-S., Parshley, S. C., Nelson, M. J., Martinache, F., & Gull, G. E. 2008, in Ground-based and Airborne Instrumentation for Astronomy II, ed. I. S. McLean & M. M. Casali, Vol. 7014, 70140X
- Ireland, M. J., Kraus, A., Martinache, F., Lloyd, J. P., & Tuthill, P. G. 2008, *ApJ*, 678, 463
- Jones, H. R. A., Longmore, A. J., Allard, F., & Hauschildt, P. H. 1996, *MNRAS*, 280, 77
- Koornneef, J. 1983, *A&A*, 128, 84
- Lloyd, J. P., Martinache, F., Ireland, M. J., Monnier, J. D., Pravdo, S. H., Shaklan, S. B., & Tuthill, P. G. 2006, *ApJ*, 650, L131
- López-Santiago, J., Montes, D., Crespo-Chacón, I., & Fernández-Figueroa, M. J. 2006, *ApJ*, 643, 1160
- Martinache, F., Lloyd, J. P., Ireland, M. J., Yamada, R. S., & Tuthill, P. G. 2007, *ApJ*, 661, 496
- McCarthy, Jr., D. W., Henry, T. J., Fleming, T. A., Saffer, R. A., Liebert, J., & Christou, J. C. 1988, *ApJ*, 333, 943

- Monet, D. G., Levine, S. E., Canzian, B., Ables, H. D., Bird, A. R., Dahn, C. C., Guetter, H. H., Harris, H. C., Henden, A. A., Leggett, S. K., Levison, H. F., Luginbuhl, C. B., Martini, J., Monet, A. K. B., Munn, J. A., Pier, J. R., Rhodes, A. R., Rieke, B., Sell, S., Stone, R. C., Vrba, F. J., Walker, R. L., Westerhout, G., Brucato, R. J., Reid, I. N., Schoening, W., Hartley, M., Read, M. A., & Tritton, S. B. 2003, *AJ*, 125, 984
- Muirhead, P. S., Erskine, D. J., Edelstein, J., Barman, T. S., & Lloyd, J. P. 2008, in *Precision Spectroscopy in Astrophysics*, ed. N. C. Santos, L. Pasquini, A. C. M. Correia, & M. Romaniello, 303–304
- Nakajima, T., Kulkarni, S. R., Gorham, P. W., Ghez, A. M., Neugebauer, G., Oke, J. B., Prince, T. A., & Readhead, A. C. S. 1989, *AJ*, 97, 1510
- Nakajima, T., Oppenheimer, B. R., Kulkarni, S. R., Golimowski, D. A., Matthews, K., & Durrance, S. T. 1995, *Nature*, 378, 463
- Paczynski, B. 1986, *ApJ*, 304, 1
- Pravdo, S. H. & Shaklan, S. B. 1996, *ApJ*, 465, 264
- Pravdo, S. H., Shaklan, S. B., Henry, T., & Benedict, G. F. 2004, *ApJ*, 617, 1323
- Racine, R., Walker, G. A. H., Nadeau, D., Doyon, R., & Marois, C. 1999, *PASP*, 111, 587
- Readhead, A. C. S., Nakajima, T. S., Pearson, T. J., Neugebauer, G., Oke, J. B., & Sargent, W. L. W. 1988, *AJ*, 95, 1278
- Reid, I. N., Gizis, J. E., & Hawley, S. L. 2002, *AJ*, 124, 2721
- Reid, I. N., Hawley, S. L., & Gizis, J. E. 1995, *AJ*, 110, 1838
- Rojas-Ayala, B. & Lloyd, J. P. 2008, in "Metallicities of M dwarfs: J and K bands" presented at the 15th Cambridge Workshop on Cool Stars, Stellar Systems, and the Sun.
- Sembach, K. R. & Savage, B. D. 1992, *ApJS*, 83, 147
- Tuthill, P., Lloyd, J., Ireland, M., Martinache, F., Monnier, J., Woodruff, H., ten Brummelaar, T., Turner, N., & Townes, C. 2006, in *Advances in Adaptive Optics II*. Edited by Ellerbroek, Brent L.; Bonaccini Calia, Domenico. *Proceedings of the SPIE*, Volume 6272, pp. (2006).
- Tuthill, P. G., Monnier, J. D., Danchi, W. C., Wishnow, E. H., & Haniff, C. A. 2000, *PASP*, 112, 555
- Vacca, W. D., Cushing, M. C., & Rayner, J. T. 2003, *PASP*, 115, 389
- Valenti, J. A. & Fischer, D. A. 2005, *ApJS*, 159, 141
- van de Kamp, P. 1971, *ARA&A*, 9, 103
- Weis, E. W. 1996, *AJ*, 112, 2300
- Wilson, J. C., Henderson, C. P., Herter, T. L., Matthews, K., Skrutskie, M. F., Adams, J. D., Moon, D.-S., Smith, R., Gautier, N., Ressler, M., Soifer, B. T., Lin, S., Howard, J., LaMarr, J., Stolberg, T. M., & Zink, J. 2004, in *Presented at the Society of Photo-Optical Instrumentation Engineers (SPIE) Conference*, Vol. 5492, *Ground-based Instrumentation for Astronomy*. Edited by Alan F. M. Moorwood and Iye Masanori. *Proceedings of the SPIE*, Volume 5492, pp. 1295-1305 (2004)., ed. A. F. M. Moorwood & M. Iye, 1295–1305